RSC Advances

PAPER

View Article Online
View Journal | View Issue

Cite this: *RSC Adv.*, 2020, **10**, 19425

A fluorescent microsensor for the selective detection of bifenthrin

Xiaodong Lv *[a] and Peng Gao[b]

Based on the fluorescence quenching phenomenon, a smart fluorescent microsensor was synthesized. The bifenthrin (BI) microsensor inherited the high selectivity of molecular imprinted polymers (MIPs) and the excellent fluorescence properties of aqueous CdTe quantum dots (QDs). Aqueous CdTe QDs are functionalized by octadecyl-4-vinylbenzyl-dimethyl-ammonium chloride (OVDAC). A type of functional monomer, 4-vinylphenylboronic acid (VPBA), was used and its boronic acid groups could covalently combine with a *cis*-diol compound for direct imprinting polymerization. The OVDAC-functionalized aqueous CdTe QDs were used as solid supports and auxiliary monomers. Under optimal conditions, experimentation showed that BI had a linear detection range of 10 to 300 μmol L^{-1} with a correlation coefficient of 0.9968 and a high imprinting factor (IF) of 4.53. In addition, the prepared MIP-OVDAC/CdTe QDs were successfully used to detect BI in water samples. Therefore, this work provided a highly selective and sensitive fluorescence probe for the detection of BI. In addition, the fluorescence probe could be used to detect other targets by changing the functional monomers.

Received 23rd March 2020
Accepted 7th May 2020

DOI: 10.1039/d0ra02658a

rsc.li/rsc-advances

Introduction

A sensor[1] is an intelligent information interaction platform, which is associated with analog-to-digital conversion. Its aim is to parameterize a model through collecting and processing data. In particular, microsensors,[2–4] a new generation device, is more and more popular due to its miniaturization and integration. Quantum dots (QDs),[5–7] also called semiconductor nanocrystals, have distinct photoelectric advantages, such as controllable emission wavelength, narrow and symmetric emission spectrum, high luminescence efficiency and anti-drift of light. Based on an electron-transfer mechanism between a target and QDs, QDs have been used as optical sensors of various analytes including ions, small molecules and biological macromolecules.[8–10]

In traditional agricultural industries, bifenthrin (BI),[11–13] a type of artificially synthesized pyrethroid insecticide, is widely applied. Because of pesticide residues in soils, lakes and so on, it poses a threat to the natural environment. Hence, simple, fast and accurate detection of BI is very significant in the prevention of pollution and checking the BI-related living environment. To date, many methods, such as chromatography and electrochemistry,[13,14] have been developed to detect BI. Among these methods, QDs, and optical microsensors, have been extensively studied due to their rapid response, low cost and operability. Therefore, it is necessary to develop a novel fluorescence (FL) BI microsensor with the same advantages.

The detection of BI, is mainly based on functionalized QDs, leading to a quenching interaction between QDs and BI. However, during experiments, it was found that there are various kinds of interference from other pyrethroids structurally similar to BI and this would lead to low selectivity and inaccurate results. To improve selectivity and accuracy of a BI microsensor, the molecular imprinting technique (MIT)[15,16] was explored using functionalized QDs.

In recent years, MIT, because of its effectivity, has been widely used to guide the synthesis of molecular imprinted polymers (MIPs). MIPs have been applied to various fields,[17–19] including solid phase extraction, chemical sensors, simulation of drug analysis and so on, because of their specific selectivity, applicability and predetermined responses. So far, there are many methods[20,21] for the synthesis of MIPs. The main steps are as follows: pre-polymerization between a template molecule and a functional monomer, copolymerization in the presence of a crosslinker, and removal of the template molecule. After removing the template molecule, the MIPs are obtained, with three-dimensional specific binding sites which are perfectly complementary to the template molecule. Therefore, a target microsensor is established. Because of the existence of the recognition sites, the MIPs exhibit high selectivity and sensitivity. So far, QD@MIPs, which integrate the excellent optical property of QDs and the high selectivity of MIPs, are widely used by researchers and have proved to be an effective means of analytical detection.[22–24] However, reports about MIP-based QDs used to detect BI are very rare.

[a]*School of Electrical Engineering and Control Science, Nanjing Tech University, Nanjing 211899, China. E-mail: lvlvxiaodong@126.com*
[b]*School of Electrical Engineering, Tongling University, Tongling 244000, China*

As is known, hydrophobic CdTe QDs are widely applied in the preparation of MIPs, because hydrophobic CdTe QDs can be directly mixed with monomers for polymerization. However, synthetic MIPs typically exhibit poor FL transparency. Therefore, synthesizing high-performance CdTe QD@MIPs is very important for improving the accuracy of the detection results. According to some studies,[25,26] the aqueous phase CdTe QDs can be functionalized by the surfactant octadecyl-4-vinylbenzyl-dimethyl-ammonium chloride (OVDAC), which are then transformed into the hydrophobic CdTe QDs. The OVDAC-functionalized CdTeo QDs show high-performance FL properties and good stability. In addition, compared with hydrophobic CdTe QDs, the OVDAC-functionalized CdTe QDs exhibit better FL and transparency in the MIPs. Hence, OVDAC was used to modify the aqueous phase CdTe QDs reported in this paper.

In this work, novel MIPs based on OVDAC-modified CdTe QDs were developed and applied as a FL microsensor for selective detection of BI. Hence, to improve the effect of the MIP sensing system, 4-vinylphenylboronic acid (VPBA) was selected as a functional monomer for the detection of BI. The VPBA has a boronic acid group, which forms covalent interactions with the *cis*-diols, and directs the imprinting process. In addition, compared with other boronic acid derivatives, VPBA could participate in the polymerization *via* its *p*-vinylbenzyl groups. However, because of the high selectivity and stable three-dimensional structure of MIPs and the excellent FL property of CdTe QDs, the MIPs-OVDAC/CdTe QDs showed high selectivity, sensitivity and good stability for the BI microsensor. Finally, the strong FL of the aqueous CdTe QDs was inherited from the resultant MIPs because of the CdTe QDs modification by OVDAC, and the OVDAC-functionalized aqueous CdTe QDs were used as the solid supports and auxiliary monomers. The morphology, characterisation, optical stability and selective recognition of BI microsensors were investigated. Moreover, the prepared BI microsensor was successfully applied for the of detection of BI in real samples.

Experimental

Reagents and chemicals

All reagents used in this work were of analytical grade purity. OVDAC was purchased from the TCI (Shanghai) Development Co., Ltd. The VPBA, thioglycolic acid (TGA, 98%), $CdCl_2 \cdot 2.5H_2O$ (99.99%), tellurium powder (~100 mesh, 99.99%), $NaBH_4$ (99%), acrylamide (AM), 2,2′-azobis(2-methylpropionitrile) (AIBN), ethylene glycol dimethacrylate (EGDMA), cyhalothrin, cypermethrin, fenvalerate, BI and catechol were all purchased from the Aladdin Reagent Co., Ltd. (Shanghai, China). Ethanol and chloroform were obtained from the Sinopharm Chemical Reagent Co., Ltd. (Shanghai, China). Double distilled water (DDW) was used throughout.

Instrumentation

The morphology was obtained by transmission electron microscopy (TEM, Jeol, JEM-2100). The FL measurements were performed by on a Cary Eclipse spectrofluorometer (Agilent, USA), equipped with a plotter unit and a quartz cell. Infrared spectra (4000 to 400 cm^{-1}) were obtained by using KBr disks with a FT-IR spectrophotometer (NEXUS 470, Nicolet, USA).

Synthesis of CdTe QDs

The CdTe QDs were synthesized according to a previously reported method.[27–29] Firstly, 0.06 g of $NaBH_4$ and 0.051 g of tellurium powder were dissolved in a flask with 2.0 mL of DDW. The flask was placed in a sonicator until a uniform NaHTe solution was obtained. The prepared NaHTe solution was transferred to the mixed solution of $CdCl_2$ and TGA at pH 11.2 under N_2. The mole ratio of Cd^{2+} : TGA : HTe^- was 1 : 2.4 : 0.5. Then, the reaction mixture was refluxed at 100 °C in a water bath. The different sizes of CdTe QDs could be obtained by controlling the reflux time. The green CdTe QDs, with a size of approximately 2.0 to 3.0 nm, were used in this research.

Synthesis of OVDAC/CdTe QDs

The aqueous CdTe QDs were modified using OVDAC. Firstly, 6.0 mg of OVDAC was added to 3.0 mL of aqueous CdTe QD solution (8.0 mol L^{-1} Cd^{2+}) under vigorous stirring. Subsequently, 3.0 mL of chloroform was added into the mixture to extract the OVDAC-coated CdTe QDs. Then the chloroform phase was separated. Finally, the OVDAC-modified CdTe QDs (OVDAC/CdTe QDs) were obtained and stored for further use.

Synthesis of MIP-OVDAC/CdTe QDs

The MIP-OVDAC/CdTe QDs were synthesized *via* a precipitation polymerization method. In the process of synthesis, VPBA, AM, EGDMA and AIBN were used as auxiliary monomer, functional monomer, crosslinking agent and initiator, respectively. The OVDAC/CdTe QDs (1.0 mL), 60 mL of ethanol, 13.2 mg of Am, 40 mg of VPBA, 8.0 mg of BI, 176 μL of EGDMA and 7.5 mg of AIBN were successively added to a 100 mL flask, and the mixture was purged with N_2 for 30 min. Finally, the flask was transferred to a water bath shaker. After pre-polymerization at 50 °C for 6.0 h and copolymerization at 60 °C for 24 h, the reaction was completed, and then the mixture was centrifuged and washed several times with ethanol, and the MIP-OVDAC/CdTe QDs were obtained. The non-imprinted polymers based on CdTe QDs (NIP-OVDAC/CdTe QDs) were prepared under the same conditions but without the addition of BI.

Measurement procedure

Firstly, the prepared MIP and NIP-OVDAC/CdTe QDs were dispersed in DDW to obtain the stock solution (500 mg L^{-1}). The BI, cyhalothrin, cypermethrin and fenvalerate were dissolved separately in DDW to obtain the target solution (10 mol L^{-1}). Then, the appropriate volume of MIP or NIP-OVDAC/CdTe QDs solution and a specific amount of target solution was successively added to a 10 mL colorimetric tube. The mixture was diluted to the mark with DDW and mixed thoroughly by shaking. Finally, some of the solution was transferred to a quartz cell to carry out the FL tests after the reaction was sufficiently completed. In the experiments, all the

FL measurements were performed under the same conditions: the slit widths of the excitation and emission were both 10 nm, the photomultiplier tube voltage was set at 700 V, and the excitation wavelength was set at 330 nm with the fluorescence spectra recorded in the range of 450 to 650 nm.

Results and discussion

Preparation and characterization of MIP-OVDAC/CdTe QDs

As is shown in Fig. 1, the MIP-OVDAC/CdTe QDs were synthesized *via* precipitation polymerization. Firstly, the aqueous CdTe QDs were modified by OVDAC. Due to the long hydrocarbon chain in OVDAC, aqueous CdTe QDs could be converted to an oil phase and extracted into organic solvents. Then, the boric acid groups in the VPBA could covalently form the pentagon complex with a *cis*-diol compound, for the direct imprinting polymerization. In the presence of AM, EGDMA and AIBN, polymerization occurred *via* the *p*-vinylbenzyl groups of VPBA and OVDAC/CdTe QDs. After the removal of the target molecule BI, the MIP-OVDAC/CdTe QDs with a large number of recognition sites were prepared. Thus, when encountering BI, MIP-OVDAC/CdTe QDs would show high selectivity. This phenomenon can be explained in two ways. Firstly, the recognition sites could selectively rebind the template molecule due to the perfect complementation between the recognition sites and the target molecule in size, shape and chemical structure. Secondly, the interaction between the MIP-OVDAC/CdTe QDs and BI was covalent, which could greatly increase the selectivity of the BI microsensors.

The morphology of MIP-OVDAC/CdTe QDs was examined by TEM. As shown in Fig. 2, the diameter of the MIP-OVDAC/CdTe QDs was about 130 nm and the CdTe QDs were surrounded by a layer of shell, which was a highly crosslinked construction. These phenomena were the same as predicted earlier in the research, indicating that the experiment was feasible.

To characterize the composition of MIP-OVDAC/CdTe QDs, the FT-IR spectra of the MIP-OVDAC/CdTe QDs (Fig. 3a, curve 1) and the NIP-OVDAC/CdTe QDs (Fig. 3a, curve 2) were recorded. As is shown in Fig. 3a, the MIP-OVDAC/CdTe QDs and NIP-OVDAC/CdTe QDs showed a similar wave shape. The characteristic peaks at 1226 cm^{-1}, 1151 cm^{-1} (C–O–C stretching) and 1731 cm^{-1} (C=O stretching) were attributed to the crosslinker

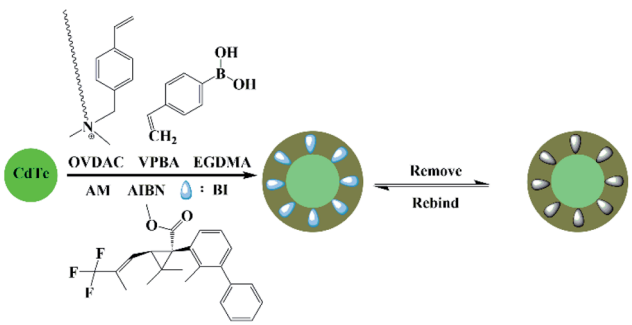

Fig. 1 A schematic illustration showing the preparation of MIP-OVDAC/CdTe QDs.

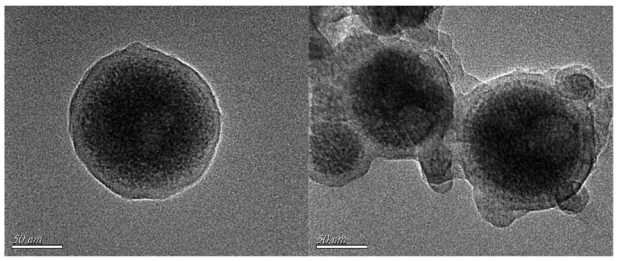

Fig. 2 TEM images of MIP-OVDAC/CdTe QDs.

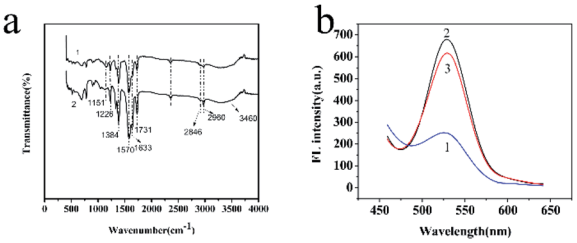

Fig. 3 (a) FT-IR spectra of MIP-OVDAC/CdTe QDs (curve 1) and NIP-OVDAC/CdTe QDs (curve 2). (b) FL spectra of BI@MIP-OVDAC/CdTe QDs (curve 1), MIP-OVDAC/CdTe QDs (curve 2), and NIP-OVDAC/CdTe QDs (curve 3).

(EGDMA). The characteristic peaks at 1384 cm^{-1}, 3460 cm^{-1} and 1633 cm^{-1} were attributed to the stretch of C–N, and the stretching and bending vibration of the secondary amine groups of the functional monomer (AM), respectively. Moreover, the characteristic peaks about the $-CH_2-$ vibration (2960 cm^{-1} asymmetric stretching vibration, 2846 cm^{-1} symmetric stretching vibration) are also shown in Fig. 3a, indicating the existence of OVDAC-coated CdTe QDs in the polymers. All the results suggest that MIP-OVDAC/CdTe QDs and NIP-OVDAC/CdTe QDs have been successfully prepared.

The excellent fluorescence property of MIP-OVDAC/CdTe QDs was demonstrated by comparing the FL spectra. As is shown in Fig. 3b, the FL intensity of MIP-OVDAC/CdTe QDs was weak at the beginning, but it was quickly recovered after the removal of BI. This indicated that the template molecules can be eluted from the MIPs by a simple method. In addition, the MIP-OVDAC/CdTe QDs were dissolved in DDW, exhibiting a strong green fluorescence under UV excitation with a wavelength of 365 nm.

Effects of pH, solution concentration and time

In any experiments, changes of the external factors may cause an inaccurate result. Therefore, the various factors affecting the BI microsensors were studied and optimized, including pH, solution volume and response time.

The pH value was significant to the FL intensity of the BI microsensors. As is shown in Fig. 4a, when the pH value was between 3.0 and 7.0, the relative FL intensity of the MIP-OVDAC/CdTe QDs drastically changed. The pH was between 7 and 12, the relative FL intensity of the MIP-OVDAC/CdTe QDs changed little. In addition, the relative FL intensity of the MIP-OVDAC/

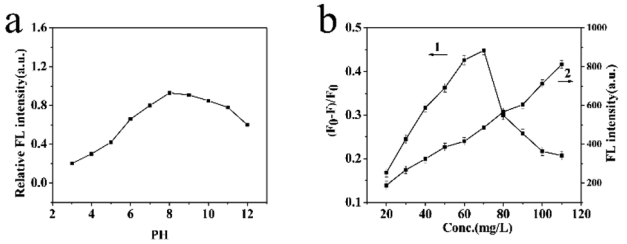

Fig. 4 (a) Effect of pH on the FL intensity of MIP-OVDAC/CdTe QDs. (b) The effects of the addition of MIP-OVDAC/CdTe QDs on FL intensity.

CdTe QDs was greatest at pH 8.0. Therefore, the value of 8.0 was selected as the optimal pH.

The linearity and the selectivity of the BI microsensor were impacted greatly by the volume of MIP-OVDAC/CdTe QDs. A low concentration of MIP-OVDAC/CdTe QDs would lead to a narrow linear range, whereas a high concentration of MIP-OVDAC/CdTe QDs would result in very low selectivity. Therefore, it was necessary to find a suitable volume which achieved a balance between selectivity and linearity. As is shown in Fig. 4b, the concentration range of 20 to 110 mg L^{-1} was tested and the optimum value was 80 mg L^{-1}.

The reaction time could affect the accuracy of detection results. A short reaction time would make the response inadequate, which would lead to an inaccurate result. To obtain the optimal reaction time, there were two series of experiments. One was MIP-OVDAC/CdTe QDs without any BI and the other was the MIP-OVDAC/CdTe QDs with a certain volume of BI. As is shown in Fig. 5a, the FL intensity of the MIP-OVDAC/CdTe QDs remained stable for 120 min, showing that the MIP-OVDAC/CdTe QDs were stable in the detection process. As shown in Fig. 5b, after the addition of 100 μmol L^{-1} of BI, the FL intensity of the MIP-OVDAC/CdTe QDs decreased rapidly in 20 min, and then remained unchanged. Therefore, 20 min was the ideal reaction time.

Under optimized conditions, the BI microsensor, based on the FL intensity of MIP-OVDAC/CdTe QDs, was studied further. The experiments were performed in a colorimetric tube with DDW. The mixed solution was placed at room temperature for 20 min. As a control, the NIP-OVDAC/CdTe QDs were also tested under the same conditions. As is shown in Fig. 6a and b, when BI was added linearly, the FL intensity of MIP-OVDAC/CdTe QDs

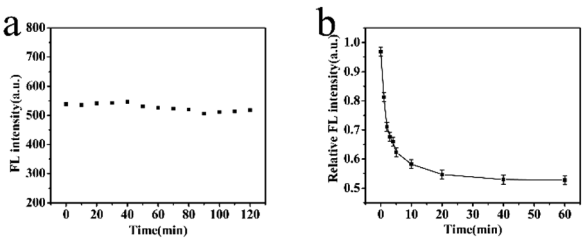

Fig. 5 (a) FL intensity change of MIP-OVDAC/CdTe QDs within 120 min. (b) FL response time of MIP-OVDAC/CdTe QDs for BI. (MIP-OVDAC/CdTe QDs: 80 mg L^{-1}).

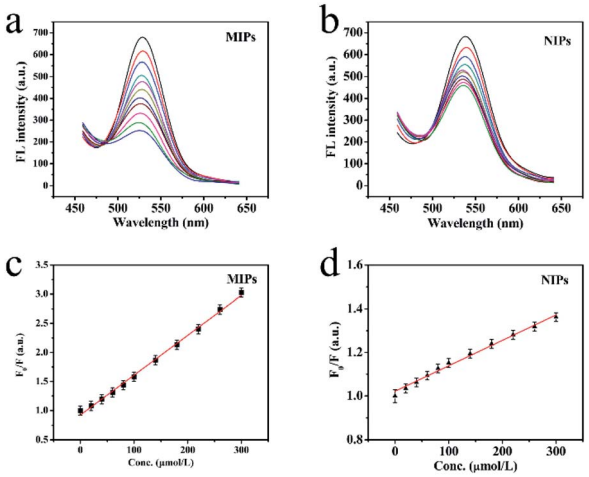

Fig. 6 (a) The FL emission spectra of MIP-OVDAC/CdTe QDs and (b) NIP-OVDAC/CdTe QDs (80 mg L^{-1}) with the addition of the indicated concentrations of BI, and (c) the Stern–Volmer plots for MIP-OVDAC/CdTe QDs and (d) NIP-OVDAC/CdTe QDs.

and NIP-OVDAC/CdTe QDs decreased accordingly. The quenching relationship of the BI microsensors could be described by the Stern–Volmer equation:[30–32]

$$\frac{F_0}{F} = 1 + K_{SV}[C]$$

where, F and F_0 are the FL intensity of the MIP-OVDAC/CdTe QDs or the NIP-OVDAC/CdTe QDs in the presence or absence of BI, respectively. The K_{SV} is the Stern–Volmer constant and [C] is concentration of BI. As is shown in Fig. 6c, it was found that $K_{SV,\ MIPs}$ was 0.00686 and the linear range was 10 to 300 μmol L^{-1} with a correlation coefficient of 0.9968. As is shown in Fig. 6d, the $K_{SV,\ NIPs}$ was 0.00117 and the linear range was also 10 to 300 μmol L^{-1} with a correlation coefficient of 0.9916. The IF, the ratio of $K_{SV,\ MIPs}$ and $K_{SV,\ NIPs}$, was calculated and its value was 4.53. In Table 1, compared with other results taken from the literature, the detection limit ($3\sigma/k$) was 0.4 μmol L^{-1}, in which k was the slope of the calibration line and σ was the standard deviation of the blank measurements ($n = 11$).

Selectivity of the BI microsensors

Several categories of pyrethroids (cyhalothrin, cypermethrin and fenvalerate) were selected as disruptors to evaluate the selectivity of the BI microsensor. As is shown in Fig. 7, the

Table 1 Comparison of testing results obtained in the research in this paper with some results in earlier reports

Method	Target	LOD	Selectivity	Reference
ic-ELISA	BI	2.16 mg L^{-1}	No	Li[33]
UPC_2	BI	20 μg L^{-1}	No	Wang[34]
ELISA	BI	0.004 mg L^{-1}	No	Hua[35]
MIPs-ATRP	BI	16.7 mg L^{-1}	Yes	Wu[36]
A BI microsensor	BI	0.4 μmol L^{-1}	Yes	This paper

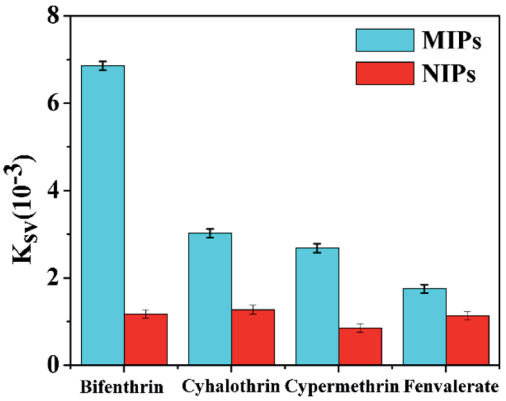

Fig. 7 Quenching constants of MIP-OVDAC/CdTe QDs and NIP-OVDAC/CdTe QDs using different kinds of pyrethroid insecticide: BI, cyhalothrin, cypermethrin and fenvalerate.

Table 2 The interference of different substances on the FL intensity of MIP-OVDAC/CdTe QDs

Coexisting substance	Coexisting concentration (μmol L^{-1})	Variable quantity of FL intensity (%)
K^+	50	1.23
Na^+	50	1.16
Ca^{2+}	20	2.46
Mg^{2+}	20	2.17
NO^{3-}	20	3.26
CO_3^{2-}	10	3.19

Table 3 Detection of BI in real samples

Sample	Concentration taken (μmol L^{-1})	Found (μmol L^{-1})	Recovery (%)	RSD (%)
0	0	0	—	—
1	50	51.34	99.48	3.50
2	100	103.12	102.12	2.31
3	150	148.03	97.63	2.19

quenching constant sequence of the MIP-OVDAC/CdTe QDs for the four compounds was as follows: BI (6.86×10^{-3}) > cyhalothrin (3.02×10^{-3}) > cypermethrin (2.68×10^{-3}) > fenvalerate (1.75×10^{-3}). As a comparison, that of the NIP-OVDAC/CdTe QDs for the four compounds was as follows: cyhalothrin (1.27×10^{-3}) > BI (1.17×10^{-3}) > fenvalerate (1.13×10^{-3}) > cypermethrin (0.85×10^{-3}). As a consequence, many tailored recognition sites had a direct impact on the selectivity of the BI microsensors. In addition, several common metal ions and anions were also used to assess the selectivity of the BI microsensor. According to the results given in Table 2, these ions had no difference on the BI microsensor. The previous results showed that the MIP-OVDAC/CdTe QDs had a higher selectivity for BI, rather than for other structural analogues. This can be explained because after the removal of the target molecule BI, the MIP-OVDAC/CdTe QDs leave many recognition sites which can selectively bind to BI.

Application in real samples

To study the feasibility of using BI microsensors in real samples, the synthetic MIPs were used to detect BI in water samples. The samples were spiked with standard BI and the results are shown in Table 3. It was found that the RSD was lower than 3.5% and the recoveries were from 97.63% to 102.12%, indicating that the MIP-OVDAC/CdTe QDs had good stability, high sensitivity and selectivity as a probe for detecting BI in real samples.

Conclusions

In summary, a BI microsensor, based on OVDAC functionalized CdTe QDs and VPBA (MIP-OVDAC/CdTe QDs), was successfully developed and applied. The boric acid group in the VPBA functionalized CdTe QDs could covalently form a pentagon complex in the *cis*-diol compound, for direct imprinting polymerization. Because of the high selectivity of the MIP and the excellent fluorescence properties of CdTe QDs, MIP-OVDAC/CdTe QDs showed high selectivity and sensitivity for detecting BI. Under optimized conditions, MIP-OVDAC/CdTe QDs were successfully used for the detection of BI in real samples. This research provides a new path that can be used to detect other targets by changing the functional monomer.

Conflicts of interest

There are no conflicts to declare and no potential interests conflicts.

Acknowledgements

This work was financially supported by the University Natural Science Foundation of Anhui Province (No. KJ2018A0476).

References

1 I. F. Akyildiz, W. Su, Y. Sankarasubramaniam and E. Cayirci, *IEEE Commun. Mag.*, 2002, **40**, 102–114.
2 S. Feng, C. Chen, W. Wang and L. J. B. Que, *Biosens. Bioelectron.*, 2018, **105**, 36.
3 X. Zhou, R. Zhang, L. Li, L. Zhang, B. Liu, Z. Deng, L. Wang and L. Gui, *Lab Chip*, 2019, **19**(5), 807–814.
4 K. Feng, J. H. Tong, Y. Wang and S. H. Xia, *Key Eng. Mater.*, 2015, **645–646**, 800–805.
5 Q. Xue, H. Zhang, M. Zhu, Z. Pei and C. Zhi, *Adv. Mater.*, 2017, **29**, 1604847.
6 F. Zhao, Y. Rong, J. Wan, Z. Hu, Z. Peng and B. Wang, *Nanotechnology*, 2018, **29**, 105403.
7 X. Qin, Y. Sui, A. Xu, L. Ling and Q. J. Xie, *J. Electroanal. Chem.*, 2018, **811**, 121–127.
8 R. Freeman, T. Finder and I. Willner, *Angew. Chem., Int. Ed.*, 2009, **48**, 7818–7821.

9 A. P. Stupak, T. Blaudeck, E. I. Zenkevich, S. Krause and C. V. Borczyskowski, *Phys. Chem. Chem. Phys.*, 2018, **20**(27), 18579–18600.
10 S. Khawas, V. Sivova, N. Anand, K. Bera, B. Ray, G. Nosal'ov and S. Ray, *Int. J. Biol. Macromol.*, 2018, **109**, 681.
11 Q. Zhang, S. Li, C. Ma, N. Wu and X. Yang, *Food Addit. Contam. A*, 2018, **53**, 1–9.
12 D. F. Frank, G. W. Miller, D. J. Harvey, S. M. Brander, J. Geist, R. E. Connon and P. J. Lein, *Aquat. Toxicol.*, 2018, **200**, 50.
13 V. J. l martínez, S. J. A. Padilla, P. Patricia, F. A. Garrido and R. G. Roberto, *J. AOAC Int.*, 2019, 6.
14 B. L. Loper and K. A. Anderson, *J. AOAC Int.*, 2019, 6.
15 Q. Rong, Y. Zhang, T. Lv, K. Shen and Q. Liu, *Nanotechnology*, 2018, **29**(14), 145503.
16 J. Wang, J. Dai, Y. Xu, X. Dai and G. Pan, *Small*, 2019, **15**, 1970006.
17 Z. Luo, A. Xiao, G. Chen, Q. Guo, Q. Chang, A. Zeng and Q. Fu, *Anal. Methods*, 2019, **11**(38), 4890–4898.
18 W. Song, Y. Chen, J. Xu, X.-R. Yang and D.-B. Tian, *J. Solid State Electrochem.*, 2010, **14**, 1909–1914.
19 P. Borunda, C. Brewer and C. Erten, *Proceedings of the 39th SIGCSE Technical Symposium on Computer Science Education, SIGCSE 2006*, Houston, Texas, USA, 2006.
20 R. F. Til, M. Alizadeh-Khaledabad, R. Mohammadi, S. Pirsa and L. D. Wilson, *Food Funct.*, 2020, **11**(1), 895–906.
21 M. Zhang, J. He, Y. Shen, W. He, Y. Li, D. Zhao and S. Zhang, *Talanta*, 2018, **178**, 1011–1016.
22 Z. A. Sun, Q. I. Yuxia, X. Wang, Y. Zhou and B. Gong, *Chin. J. Chromatogr.*, 2018, **36**, 716.
23 X. Yang, Y. Gao, Z. Ji, L.-B. Zhu and W.-W. Zhao, *Anal. Chem.*, 2019, **91**(15), 9356–9360.
24 Q. Zhao, H. Zhao, W. Huang, X. Yang and J. Wang, *Anal. Methods*, 2019, **11**(21), 2800–2808.
25 X. Wei, T. Hao, Y. Xu, K. Lu, H. Li, Y. Yan and Z. Zhou, *Sensor. Actuator. B Chem.*, 2016, **224**, 315–324.
26 L. Chang, X. He, L. Chen and Y. Zhang, *Sensor. Actuator. B Chem.*, 2017, **243**, 72–77.
27 Q. Wang, X. Wang and Y. W. J., *Photochem. Photobiol.*, 2019, **95**(3), 895–900.
28 L. Maqueira-Espinosa, R. Q. Aucelio, A. R. D. Silva and A. Pérez-Gramatges, *Colloids Surf., A*, 2018, **553**, 195–202.
29 P. Meng, Y. Xiong, Y. Wu, Y. Hu, H. Wang, Y. Pang, S. Jiang, S. Han and P. Huang, *Chem. Commun.*, 2018, **54**(42), 5342–5345.
30 A. Nitzan, J. Jortner, J. Kommandeur and E. Drent, *Chem. Phys. Lett.*, 1971, **9**, 273–278.
31 Y. Qin, Y. Zhang, S. Yan and L. Ye, *Spectrochim. Acta, Part A*, 2010, **75**, 1506–1510.
32 S. Sabury, G. S. Collier, M. N. Ericson and S. M. Kilbey, *Polym. Chem.*, 2020, **11**(4), 820–829.
33 B. Li, H. Y. Shi and M. H. Wang, *Chin. J. Anal. Chem.*, 2008, **36**, 34–38.
34 L. T. Wang, B. Wang, W. Zhou, Q. Q. Liu, S. X. Yang and Y. H. Zhang, *Chin. J. Anal. Chem.*, 2015, **43**, 1047–1052.
35 X. D. Hua, X. F. Liu, W. Yin, Y. Z. Xia, Q. J. Zhou, Y. W. Lu, W. Li, H. Y. Shi, F. Q. Liu and M. H. Wang, *Sci. Total Environ.*, 2015, **502**, 246–251.
36 X. L. Wu, X. D. Lv, J. X. Wang, L. Sun and Y. S. Yan, *Anal. Methods*, 2017, **9**, 4609–4615.